PACOSS PROGRAM STATUS AND RESULTS

K. E. Richards, Jr.
Martin Marietta Astronautics Group
Denver, Colorado

Third NASA/DoD Controls-Structures
Interaction (CSI) Technology Conference
January 2-February 2, 1989

Future large space systems (LSS), both civilian and military, will have performance objectives which require stringent pointing accuracies, relatively fast retargeting times, short settling times, accurate dynamic shape requirements, or combinations thereof. Many of these structures will be large but lightweight and will exhibit a dense, low-frequency modal spectrum with significant content within the control bandwidth.

Although it is possible in principle to achieve structural vibration control with purely active means, experience with complex structures has shown that the realities of plant model inaccuracies and real sensor and actuator dynamics frequently combine to produce disappointing results.

It has been shown (References 1-2) that a combination of passive and active control will result in a simpler system which can be expected to be more reliable and less expensive than a corresponding system utilizing active control exclusively.

The goals of the PACOSS (Passive and Active COntrol of Space Structures) program consist of a thorough investigation of the relative roles of passive and active vibration control, and the development of validated means of vibration control. (Fig. 1.)

Introduction

- Future Large Space Structures (LSS) Will Require Structural Vibration Control To Achieve Performance Goals
- Vibration Damping May Be Achieved by Passive or Active Means, or Both
- Major Goals of PACOSS Program
  - Demonstrate Roles of Passive and Active Control for Future LSS
  - Develop Means of Passive Vibration Control
  - Experimentally Verify Damping Predictions and Control Algorithms

Figure 1

The outline of this presentation is shown in Figure 2.

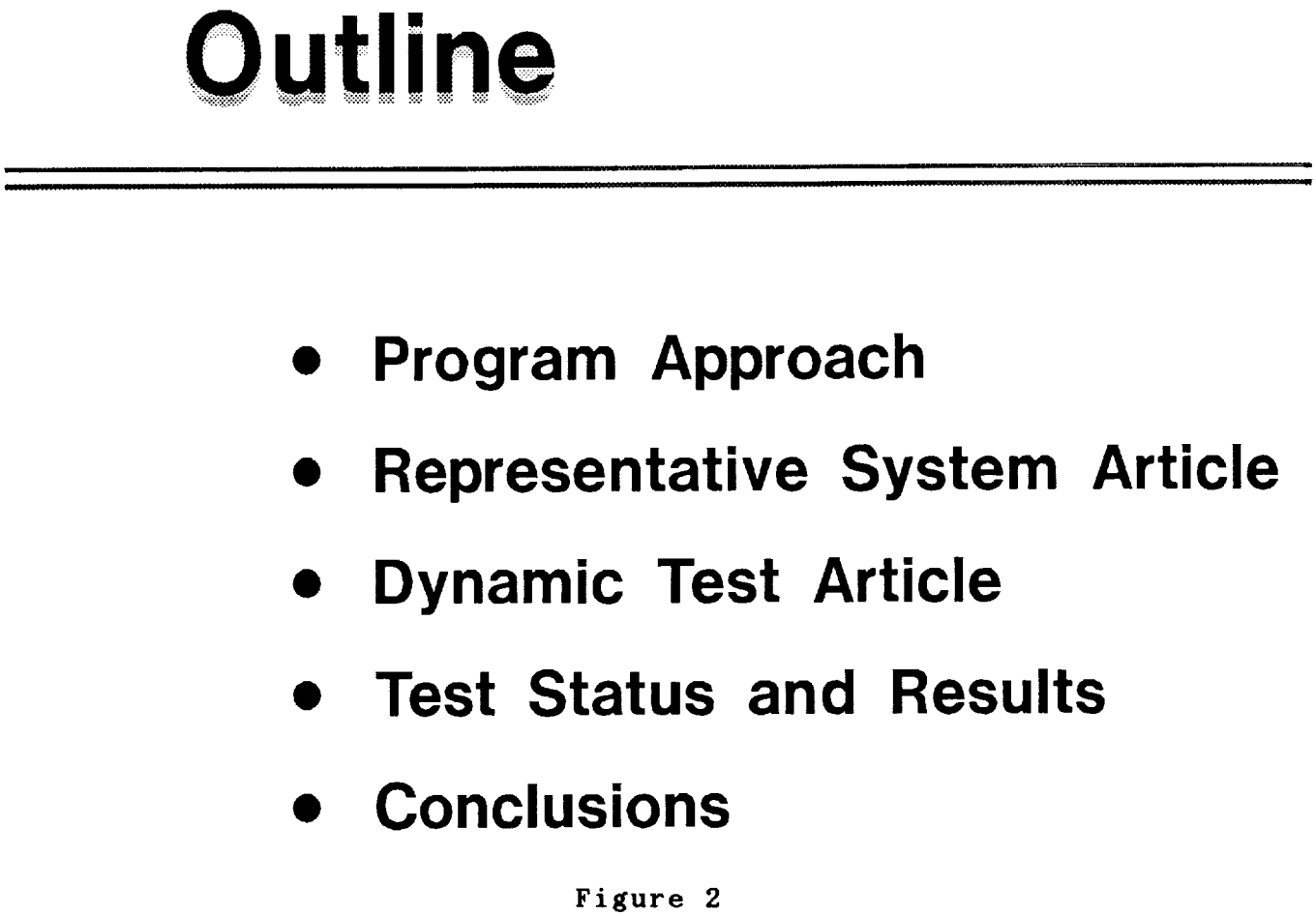

Figure 2

PACOSS, being a generic program, has as one objective to provide passive damping technology to as broad a spectrum of military and civilian large space systems as possible. Fundamental to this objective is the selection of analytic and test articles of broad applicability. These articles are then designed by analysis, and hardware components are fabricated and tested to validate design and analysis practices.

Once the hardware components are validated, substructures are designed and analyzed. These substructures are then tested to validate the higher level design and analysis practices.

Finally, the entire system is synthesized, and analytical predictions of dynamic characteristics are again validated by test. System synthesis includes active control measures as well as passive damping treatments.

The resulting technology will have broad applicability to real future space systems. Programs will be able to apply the technology with a high degree of confidence due to the careful, systematic approach applied to test hardware of a complexity similar to actual flight items. (Fig. 3.)

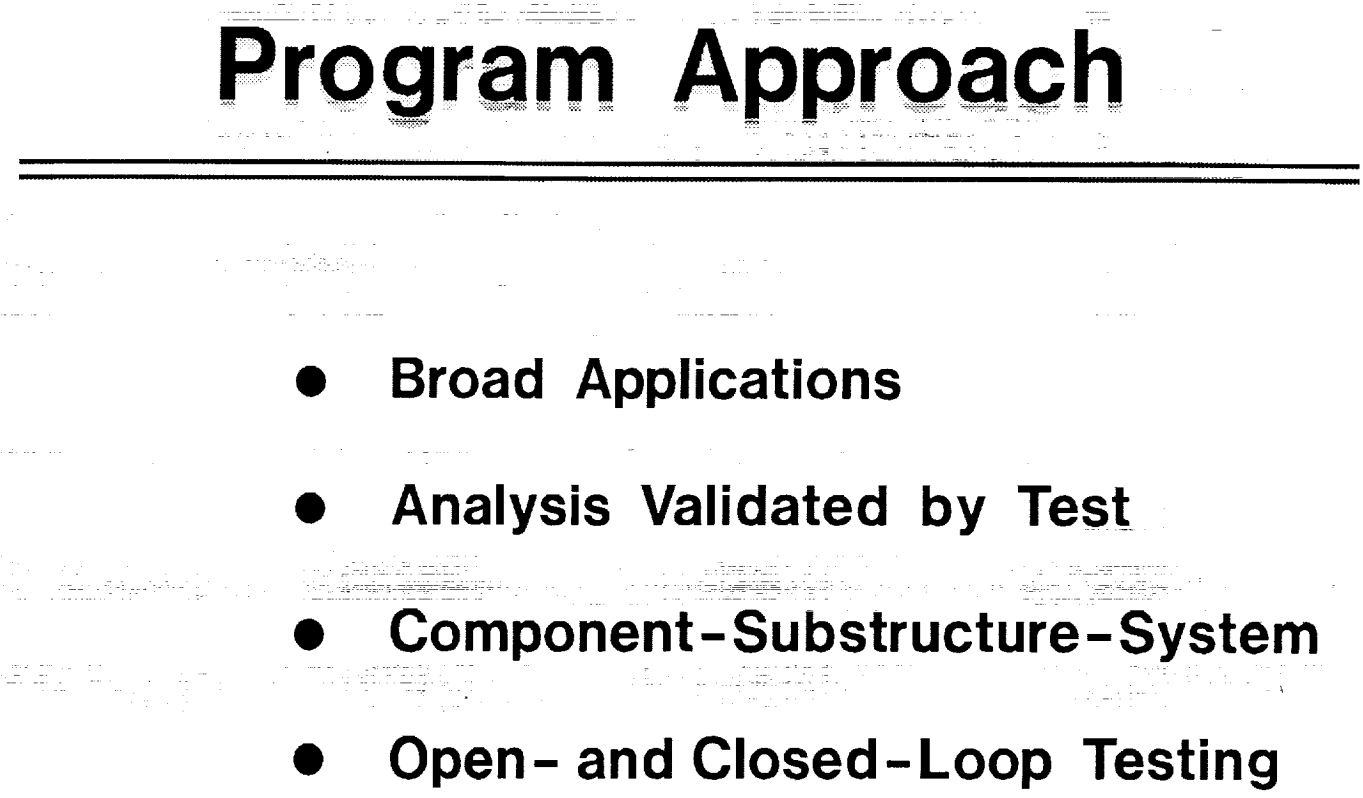

Figure 3

Figure 4 is an artist's concept of the PACOSS Representative System Article (RSA). PACOSS is a generic program, and the RSA was designed to provide an analytic test bed for system design studies that would be relevant to as many future large space systems as possible. Altogether, the RSA is traceable to 19 future systems (Reference 3).

This broad applicability was accomplished by designing a system comprised of components or substructures found on one or more future LSS. As can be seen in Figure 4, the RSA consists of seven substructures. The ring truss, 20 meters in diameter, serves as a structural "hardback" for the system. The tripod structure is part of a Cassegrain optical system and supports a secondary mirror. The box truss represents the backup structure for an optical surface. The dish antenna is for communication with the ground. The linear truss supports sensitive equipment. The two solar arrays are sized for 25 kilowatts of power.

Passive damping treatments are designed for each selected substructure. It is possible to provide passive damping treatments to all components, but it was decided not to damp the ring truss to simulate systems where some components would be unavailable for damping treatments.

The level of passive damping to be applied was based on a performance simulation of the system with various levels of passive damping (References 2,4), a technique to be followed in the design of real systems.

PACOSS RSA

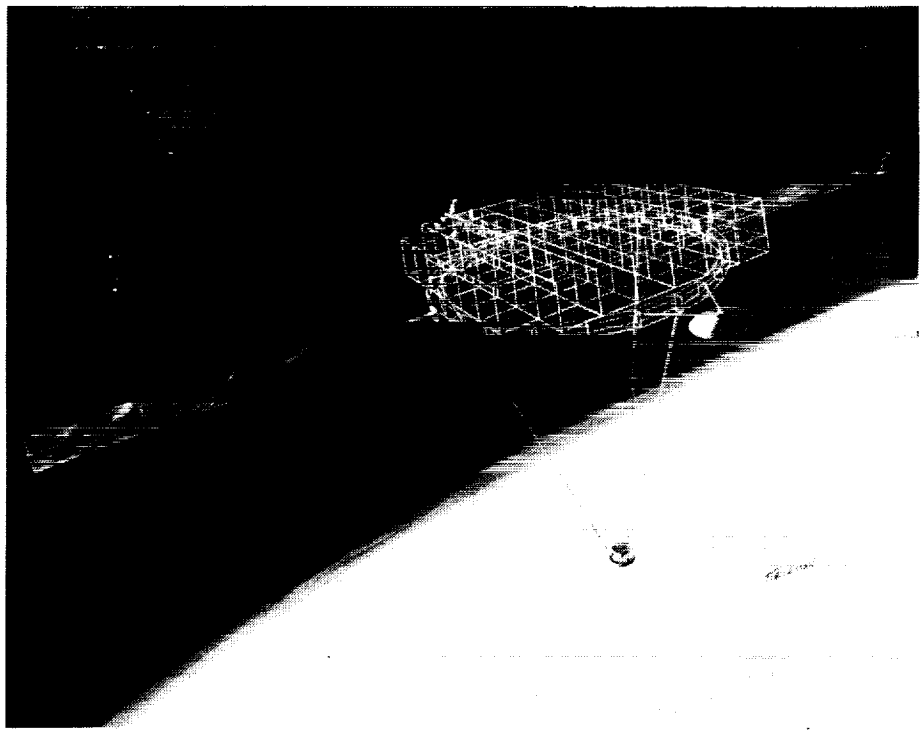

Figure 4

The DTA was designed to be dynamically similar to the RSA and is serving as a hardware validation tool for the analytic methods and design practices used to provide passive damping to realistic structures. The requirements shown in Figure 5 have been selected to assure traceability to the RSA within the realities of the test environment and budgetary constraints. It is noted that the DTA is space-qualifiable, although there are currently no plans to fly it.

Because the DTA is a validation device, it is important that no inadvertent sources of damping are present. This function was the major reason the PACOSS program chose to avoid exotic or complicated suspension techniques for the DTA. A consequence of this decision was that it was necessary to stiffen the DTA to permit it to survive the one-g test environment without extensive distributed support. This stiffening resulted in a frequency increase of approximately two Hz. The frequency shift does not compromise program objectives, however.

Dynamic Test Article (DTA) Requirements

- Validation of Damping Treatment Design and Analysis Techniques
- Dynamically Similar to RSA
- Deliverable to Orbit As Single Shuttle Payload
- Negligible Unpredicted Damping
- Suitable for 1-g Test
- Easily and Inexpensively Fabricated

Figure 5

All components of the DTA have been fabricated and tested. Figure 6 shows the sizes of the DTA structural components.

Summary of Final DTA Dimensions

Component	*Dimension, m*	*Mass, kg*
* 1) Box Truss	2.89x2.59x0.324	180.5
* 2) Ring Truss	Diameter: 2.9	59.7
* 3) Tripod	Diameter at Base: 2.59 Height: 2.59	29.9
* 4) Equipment Platform	Length: 1.295	7.04
* 5) Antenna	Diameter: 0.648	4.52
*6,7) Solar Arrays	Length: 2.59	12.0
* *Fabricated and Tested*		

Figure 6

The first component modal survey was of the ring truss (References 2,5). This substructure is the central element of the system, and it is critical that this portion of the system be modelled accurately.

Figure 7 shows the ring truss suspended in its test configuration. The truss is suspended by three lightweight cables approximately 25 feet long. Each cable was suspended from a zero spring-rate mechanism (ZSRM). This arrangement results in three virtually zero rigid-body modes and three pendulum modes of approximately 0.25 Hz for the suspension, thereby providing good separation from the flexible modes of the system.

The modelling of the interfaces between the ring truss and the remaining substructures is critical. To exercise these interfaces, thereby permitting evaluation of the accuracy of the model, the ring truss was mass-loaded at all interface points during this test.

DTA Ring Truss in Test Configuration

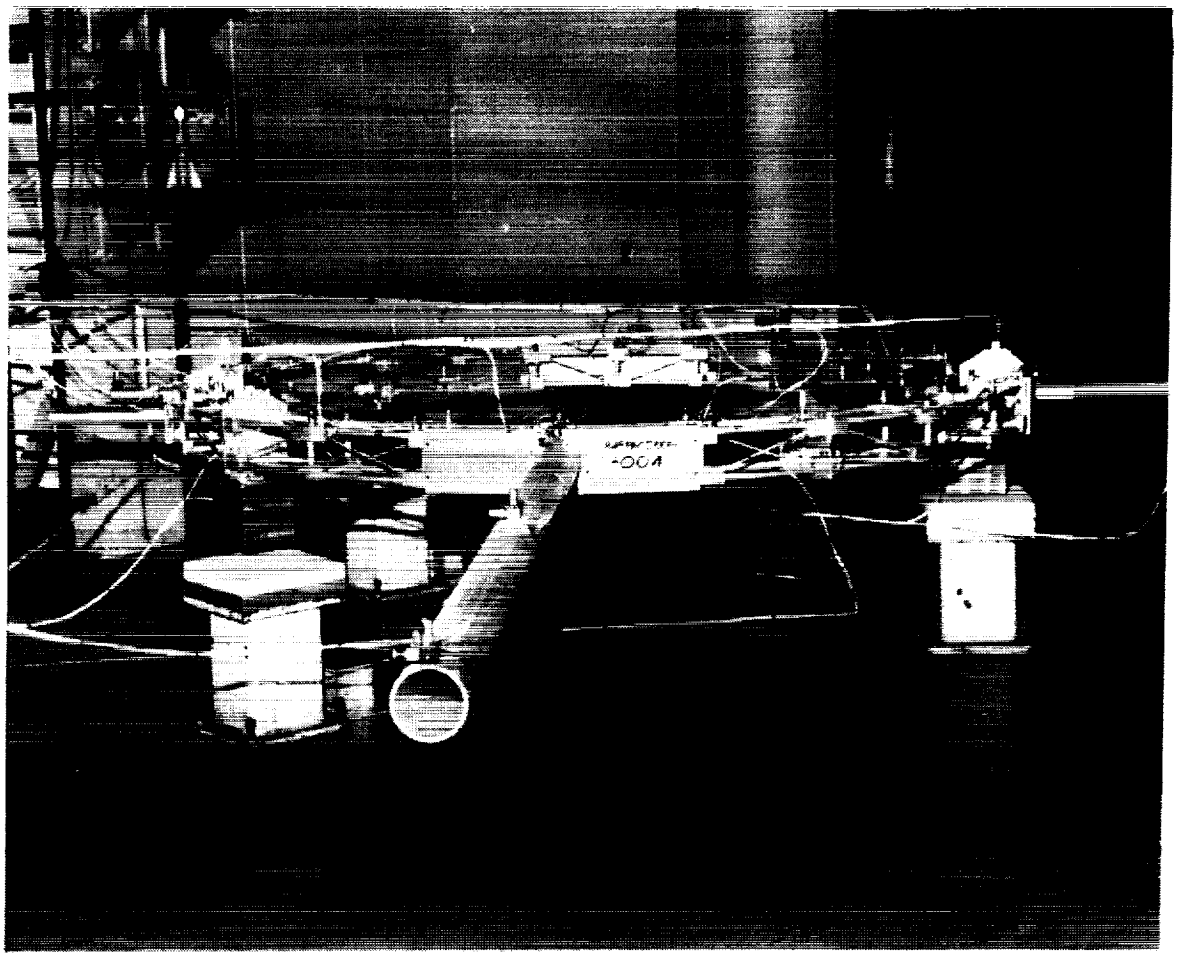

Figure 7

Figure 8 shows one of the three identical ZSRMs. The large vertical spring supports the static load due to the weight of the DTA. The position of this spring is adjusted so that the two side members, which pivot about their ends, are horizontal. The large nuts on the side members are turned to place the springs on the side members into states of equal compression.

The vertical spring and side members are connected to a common pivot point. A pair of guide rods connect this point to the DTA suspension cable. Downward displacement of the pivot results in an incremental spring force in the vertical spring, accompanied by rotations of the side members. The incremental downward forces due to the rotations of the compressed side members tend to cancel the incremental upward force in the large spring. Proper selection of the ZSRM parameters produces perfect cancellation for small displacements, resulting in a suspension with zero stiffness for the displacements normally encountered during a modal survey.

Zero Spring-Rate Mechanism

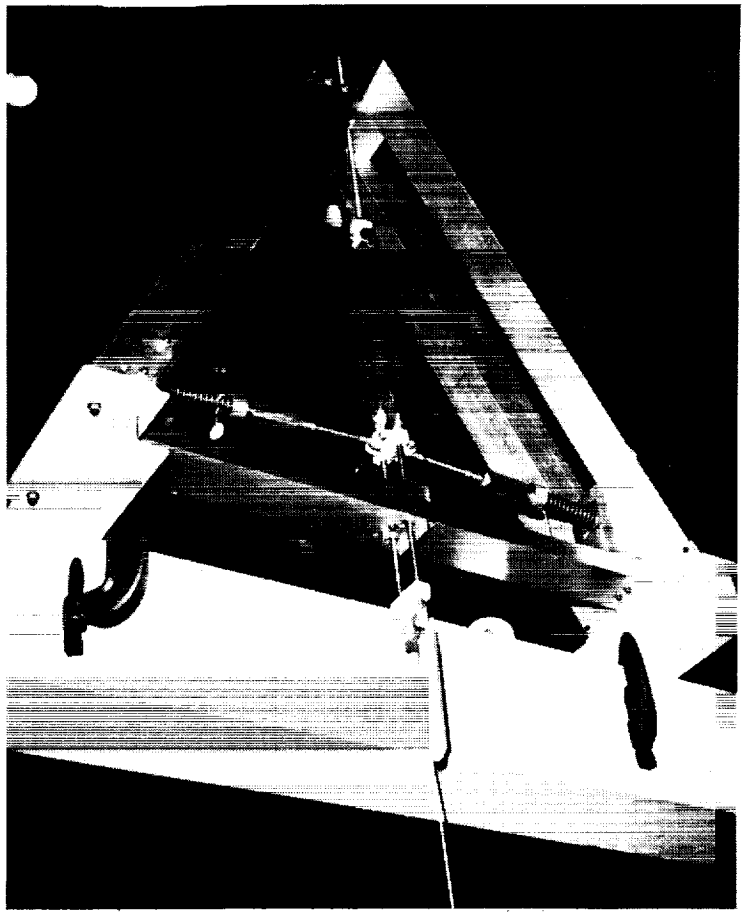

Figure 8

The results of the test and comparison with the analytic model are shown in Figure 9. Note the extremely low damping in the higher modes.

The damping values shown in this figure were obtained from tuned-decay tests, a very accurate method for those cases where damping is low and the modes can be separated. Note that the 12.5 and 12.7 Hz modes were too close in frequency to be separated well, and the 13.2 Hz mode could not be tuned. Damping values for these modes are available from the single-point random tests and have been presented elsewhere (Reference 2).

The comparatively high damping values (relative to the other modes but low in the absolute sense) for modes one and two were due to excessive wear in the mild steel ZSRM guide rods which occurred during testing. This situation was corrected by the use of case hardened rods during final testing.

Ring Truss Modal Survey—Results

f_n, Hz		ζ, %
Measured	Post Test Analytic	Measured
3.25	3.29	0.3
6.33	6.47	0.7
8.78	9.40	0.14
9.28	9.91	0.17
12.5	14.9	0.2 - 0.3
12.7	12.2	0.2 - 0.3
13.1	12.5	0.16
13.2	14.1	Not Measured
15.1	15.6	0.15

Figure 9

The tripod is shown in the test configuration in Figure 10 (References 2,5). The dark color of the legs is due to the graphite-epoxy constraining layer. Rotational shear dampers are located at each of the three interfaces between the tripod legs and the sixty pound secondary mirror. The bottoms of the tripod legs are fixed to the floor. The model assumed an effectively rigid floor, and experimental data confirmed the assumption.

DTA Tripod in Test Configuration

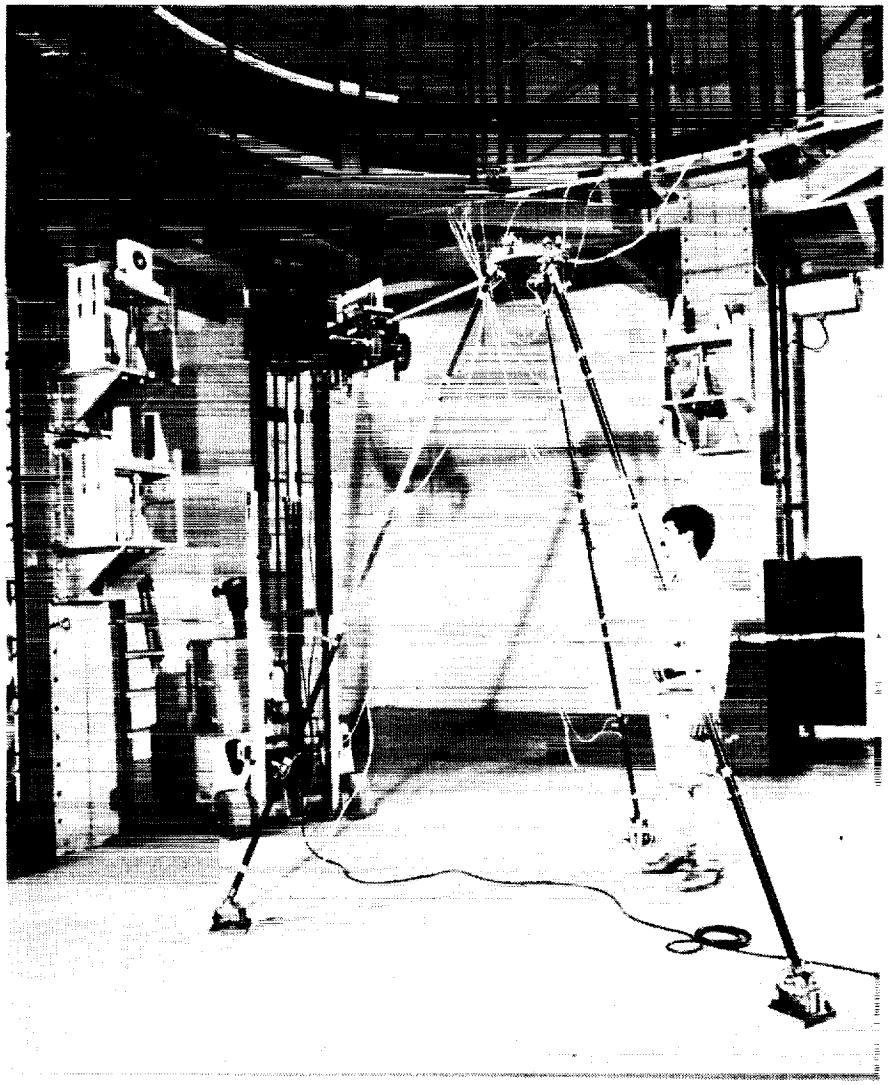

Figure 10

The details of the constrained-layer damping treatment on the tripod legs are shown in Figure 11 (Reference 4). The tubing used was aluminum. A layer of viscoelastic material is bonded to the tube and to the graphite/epoxy constraining layer. Care is used to avoid bonding adjacent constraining layers together, as this would drastically reduce the damping level.

Detail Design of Damping Treatment for DTA Tripod

- Tripod Model Predicted 5% Modal Damping Using Constrained Layer Treatment

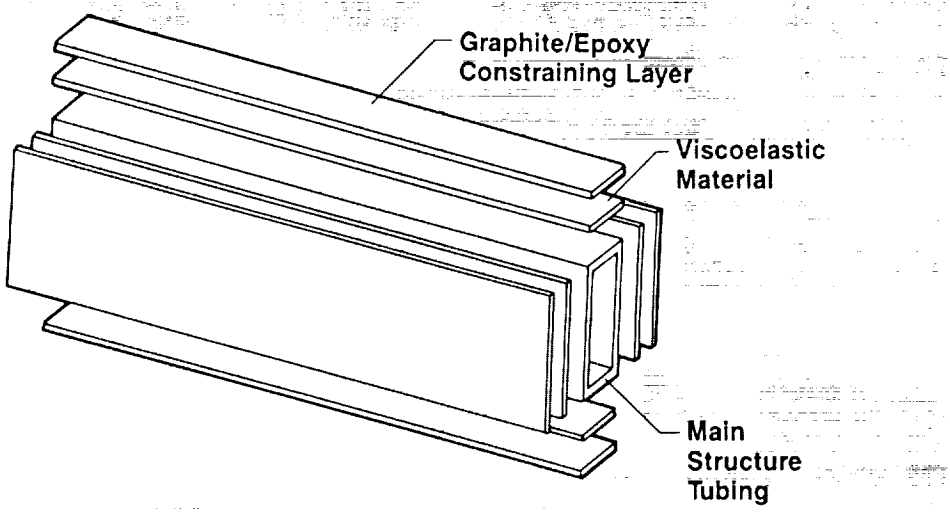

Figure 11

The details of the rotational shear damper are shown in Figure 12 (Reference 4). The damper housing is connected to the tripod legs and the damper shaft is connected to the secondary mirror. The viscoelastic material is bonded to both the shaft and housing so that relative rotation between the housing and shaft induces shear strain into the VEM (viscoelastic material).

Detail Design of Damping Treatment for DTA Tripod (cont)

- Determine Dimensions of Viscoelastic Cylinder for Chosen Material (Acrylic Core Foam)
- Design Method of Supporting Weight and Dynamic Loads in Other DOFs*

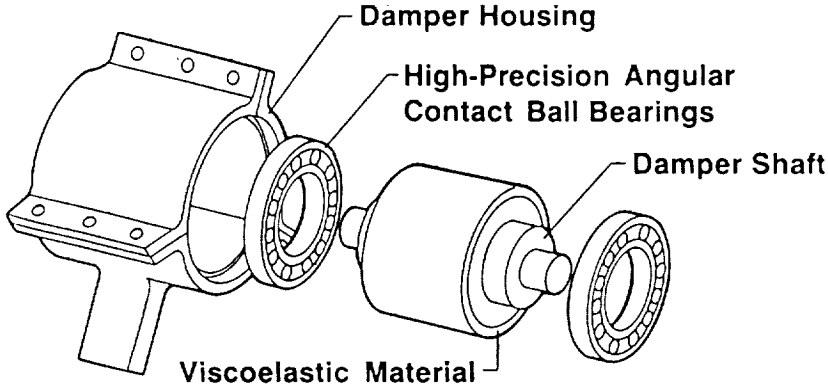

*Degree of freedom (DOF)

Figure 12

The comparison between predicted and measured frequency and damping is shown in Figure 13 (Reference 5). The predicted values were derived considering the frequency dependence of the VEM properties as well as the geometric stiffness effects induced by the weight of the heavy secondary mirror acting on the tripod legs. Note that these two effects tend to offset each other, and both must be considered if predictions are to be accurate.

VEM properties under current manufacturing standards frequently vary by 50 percent from batch to batch, so these results are exceptionally good.

Tripod Modal Survey—Results

f_n, Hz		ζ, %	
Measured	Predicted	Measured	Predicted
3.91	3.84	15.9	17.9
3.97	3.84	15.7	17.9
4.78	4.63	6.7	7.1
9.55	9.89	9.2	8.7
9.66	9.89	8.6	8.7
11.7	11.7	9.2	8.4
12.7	13.8	11.4	12.3
13.3	13.8	11.1	12.0

Figure 13

The box truss is shown in the test configuration in Figure 14. The large yellow structure is known as the "T-beam", and is part of the test facility. The box truss is clamped to the T-beam, and both the box truss and T-beam were instrumented for the test (Reference 5).

DTA Box Truss in Test Configuration

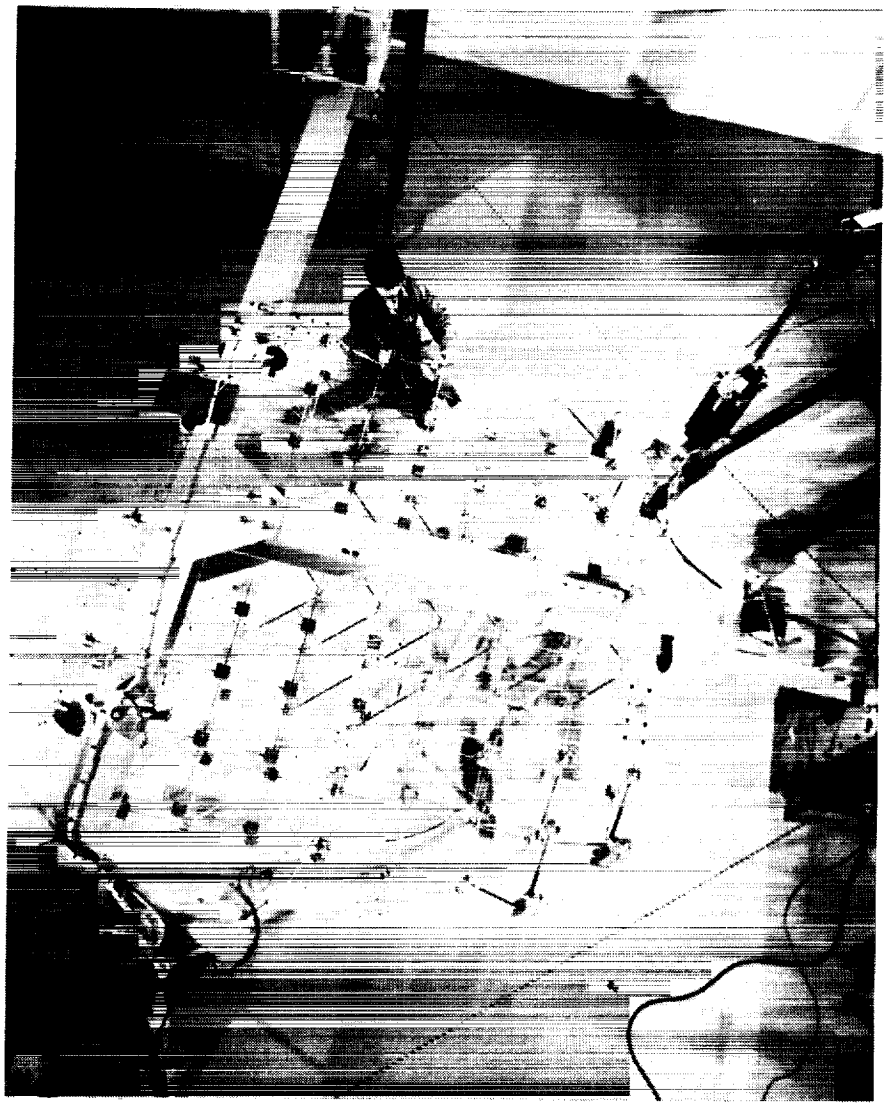

Figure 14

Figure 15 is a close-up of one corner of the box truss. The two large gray assemblies are steel thruster mass simulators weighing approximately 25 pounds each. The small grey blocks are segmented mirror mass simulators. The brass cylinders are extensional shear dampers.

The design goal was to achieve at least five percent modal damping in the first two fixed interface modes. This required damping treatment of 31 members out of more than 500. It should be noted that the truss members are highly stressed due to the large amount of non-structural mass in the one-g environment, and optimum placement of the viscoelastic dampers is not possible. To achieve the same level of damping in a zero-g environment would require only 23 damping members of much smaller size placed in more optimum positions.

Box Truss Mass Simulators

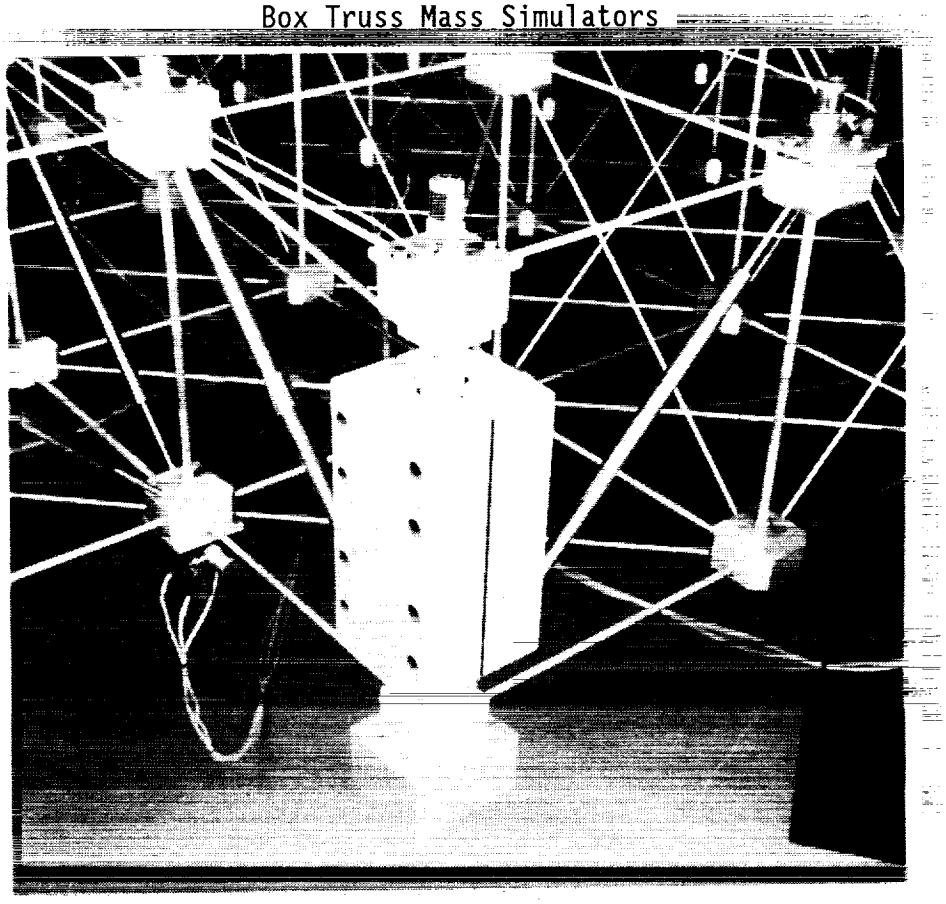

Figure 15

Details of the extensional shear dampers are shown in Figure 16 (Reference 4). The damper rods enter the box truss joint blocks. The rods are wrapped with self-adhesive VEM as shown, and the clamshells bonded to the VEM. The solid sleeve is then bonded to the clamshells. Relative extensional motion of the damper rods induces shear strain into the VEM. A parallel elastic path to control creep is provided by the helix spring. Approximately 85 percent of the strain energy in the damper in the first box truss mode is in the VEM. Thus, the efficiency of this design is 85 percent.

Extensional Shear Damper Design

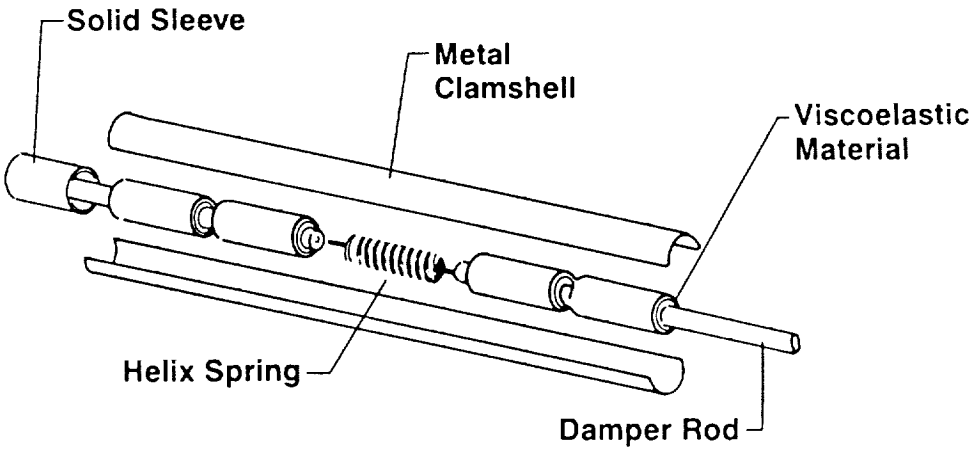

Figure 16

Figure 17 shows the analytical values for the fixed interface modal frequencies and damping ratios. The damping design goal of at least five percent modal damping in the first two fixed interface modes was met with an additional benefit in the other modes due to "damping spillover," wherein the dampers, being active in the higher modes, provide some damping to those modes.

DTA Box Truss Fixed Interface Frequencies and Damping (Analytic)

Mode No.	f_n (Hz)	ζ %
1	4.02	8.6
2	8.75	5.7
3	16.3	3.6
4	17.1	1.7
5	17.7	1.1
6	18.9	5.3

Figure 17

To construct a test fixture which would behave rigidly for the large box truss was beyond program resources. A T-beam, part of the test facility, was used for the test fixture.

The modal test results for the box truss/T-beam setup are shown in Figure 18 (Reference 5). The T-beam participated in all the modes more than anticipated, with the third system mode being principally a T-beam torsion mode. Model tuning involved only a refinement of the T-beam portion of the model. Thus, the clamped modal damping ratios shown in the Figure 17 were achieved for the box truss with fixed interfaces.

Box Truss Modal Survey - Post Test Analysis

- Third Test Mode Was I-Beam Torsion Mode
- Only Analytic Modification Was Adjustment of I-Beam Torsional Stiffness

f_n, Hz		ζ, %	
Measured	*Predicted*	*Measured*	*Predicted*
4.38	4.09	6.6	6.9
10.3	9.39	3.6	3.8
13.6	13.0	0.6	0.5
15.9	15.6	< 0.5	0.3
18.0	18.3	< 0.5	1.6
19.2	18.4	< 0.5	0.3

Figure 18

The equipment platform in the cantilevered test configuration is shown in Figure 19. The brass cylinders are extensional shear dampers similar to those in the box truss, with the exception that those in the upper and lower planes are shorter in length and, being under only light static loads, do not require springs. The large steel tip mass simulates on-board equipment.

There are two aspects of this design that require further discussion, the first being the placement of the dampers. It is obvious that a more efficient application of the dampers would be to damp those bays at and near the root of the truss. Unfortunately, in the one-g environment, the members in those bays are highly loaded. The resulting shear stresses in the VEM would exceed design limits if dampers were placed in those bays.

The next aspect is the relatively large size of the dampers. A large shear area is necessary to reduce the VEM shear stresses to an acceptable level in the one-g environment. This results in long dampers. However, merely increasing the length would result in overly stiff dampers. Increasing the diameter reduces the stiffness to the proper level.

From this discussion, it is obvious that a zero-g design would have fewer, smaller dampers more optimally placed near the root of the truss to achieve the same level of damping.

DTA Equipment Platform in Test Configuration

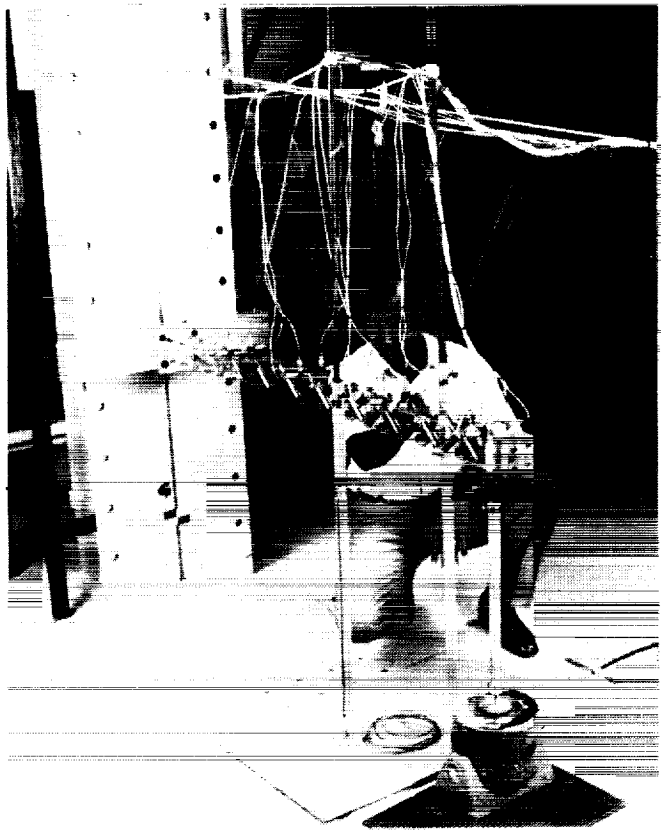

Figure 19

Results of the equipment platform are shown in Figure 20. The analytic values are derived from a model which accounts for the relatively large static deflection of the structure under the one-g loading. Failure to account for this deflection results in very poor cross-orthogonality checks between the analytic and experimental mode shapes.

As can be seen, predictions of the modal frequencies are quite good, but damping predictions are not as accurate as have been obtained for the tripod and box truss.

Mode 1 is principally a lateral bending mode, but with some torsional coupling due to the gravity-induced droop. Mode two is a bending mode in the vertical plane. Mode three is principally torsion.

In the first mode, the majority of the damping is provided by the top and bottom plane dampers. In the second mode, the side plane dampers provide virtually all the damping. The torsion mode derives its damping from all dampers. The side plane dampers are thus suspect, and it is possible that their shorter length results in significant "end-effects" of the VEM.

DTA Equipment Platform Results

Mode No.	f, Hz			ζ %		
	Test	Analytic	% Error	Test	Analytic	% Error
1	3.78	3.64	3.70	8.3	10.0	20.5
2	3.79	3.81	0.53	5.2	4.6	11.5
3	13.3	12.9	3.01	27.1	25.2	7.01

Figure 20

The DTA antenna is shown in the test configuration in Figure 21. This test setup is somewhat unique in that non-contacting proximity probes were used in place of accelerometers due to the extremely fragile nature of the dish.

The DTA antenna dish actually buckles due to gravity loads. The dish was modelled in its buckled shape, and analytic modes shapes and damping ratios were calculated. As would be expected, results were not as good as for the other structures.

A similar dish without damping treatment was fabricated and tested. That test verified that air damping was not significant.

DTA Antenna in Test Configuration

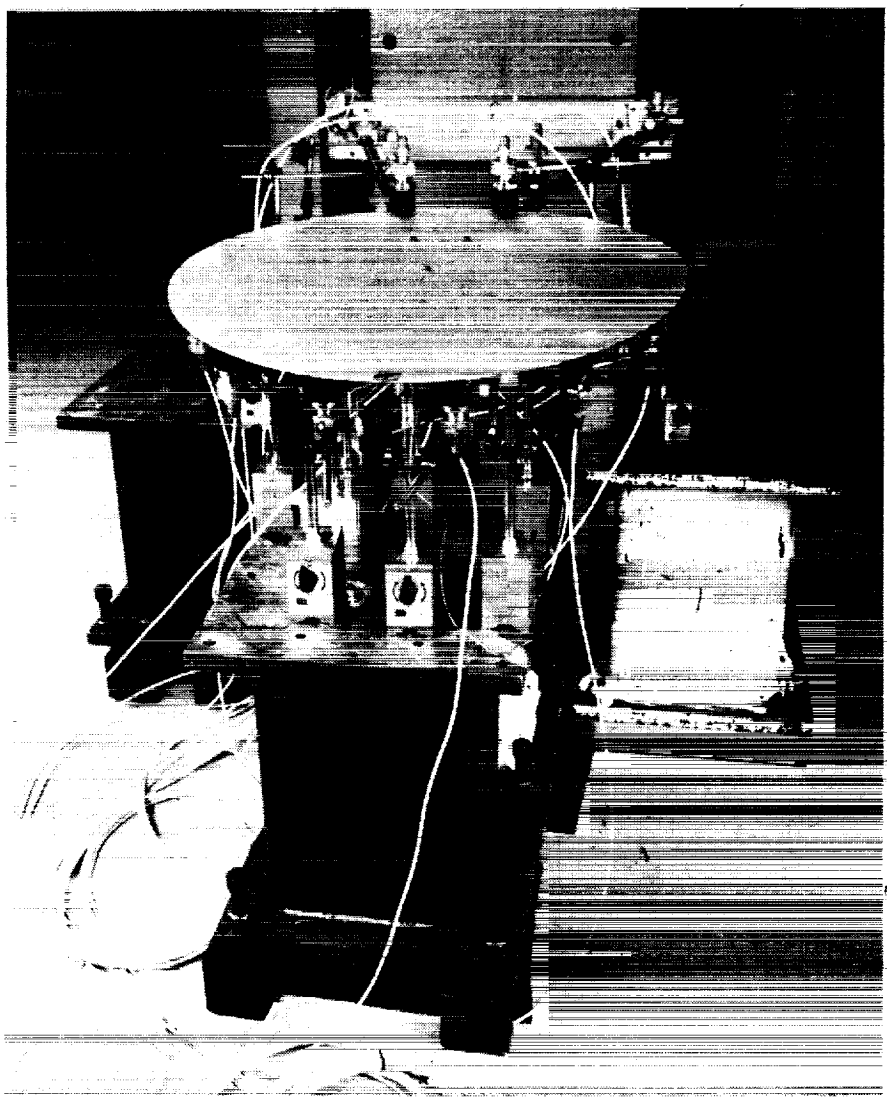

Figure 21

One of the two DTA solar arrays is shown in Figure 22. The array blanket is simulated by an aluminum gridwork to reduce air damping. The solar array mast has damping treatments similar to the tripod legs. Viscoelastic tuned mass dampers (TMDs) are placed on the fourth and seventh blanket ribs to damp the out-of-plane blanket modes. Viscoelastic shear straps were also placed at the spreader bar/blanket interfaces.

The curve in the mast illustrates the effect of the gravity field. When the deformation is accounted for, results were generally good, although the TMDs were extremely flexible and behaved nonlinearly, making prediction of blanket mode damping difficult. We note that the TMDs did provide effective blanket damping, however.

DTA Solar Array

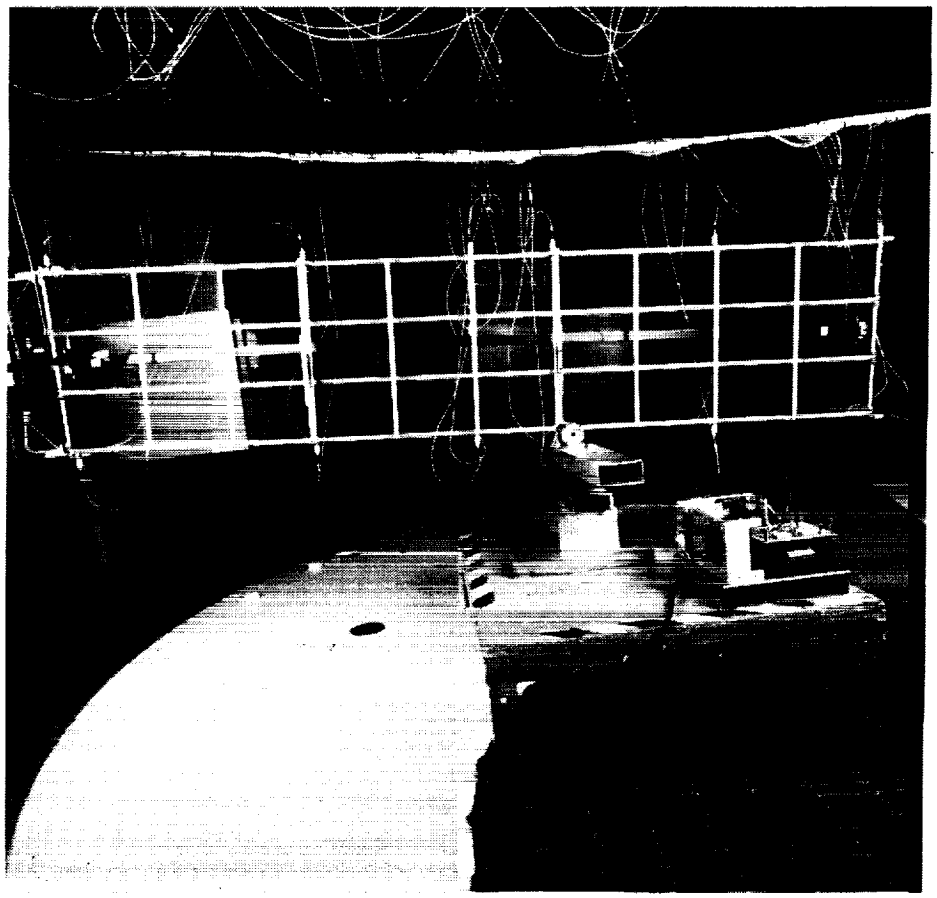

Figure 22

The PACOSS program also investigated active control of structural modes. Figure 23 shows the prototype proof-mass actuator in a bench test configuration. The power supply and the control circuits are in the background.

The actuator base is mounted, through three force gauges, to a shaker. This setup was used to validate the analytic actuator model.

Prototype Proof-Mass Actuator in Bench Test Configuration

Figure 23

Figure 24 shows details of the actuator construction. A linear motor is fastened rigidly to the thin shaft, which passes through linear bearings at the top and middle of the thirteen inch frame. The bearings were matched to the shaft by the manufacturer, resulting in a very low sliding friction. This design is somewhat unique compared to similar actuators in that there is no relative motion between the motor and the shaft, thereby eliminating eddy-current damping.

The 4.3-lb. motor is suspended on springs as a gravity offload. The springs are sized so the open-loop frequency is approximately 1.5 Hz. The larger cylinder, parallel to the motor and shaft, is an LVT which measures relative velocity between the actuator frame and the motor. The thin LVT core shaft passes through a Teflon sleeve. The LVT is used to provide damping to the actuator, and the gain on this portion of the circuit is adjustable to permit selection of the desired damping level.

An accelerometer is mounted on the top of the frame. The output from this accelerometer is integrated by a bi-quad filter (which has zero gain at DC) to provide inertial velocity to the modal controller. The actuator will act effectively as a dashpot connected between the DTA and ground.

Six of these actuators were manufactured. The weight of each actuator is approximately six pounds. These actuators, when combined with the passive damping augmentation, were designed to provide at least five percent modal damping to the targeted DTA modes.

Actuator

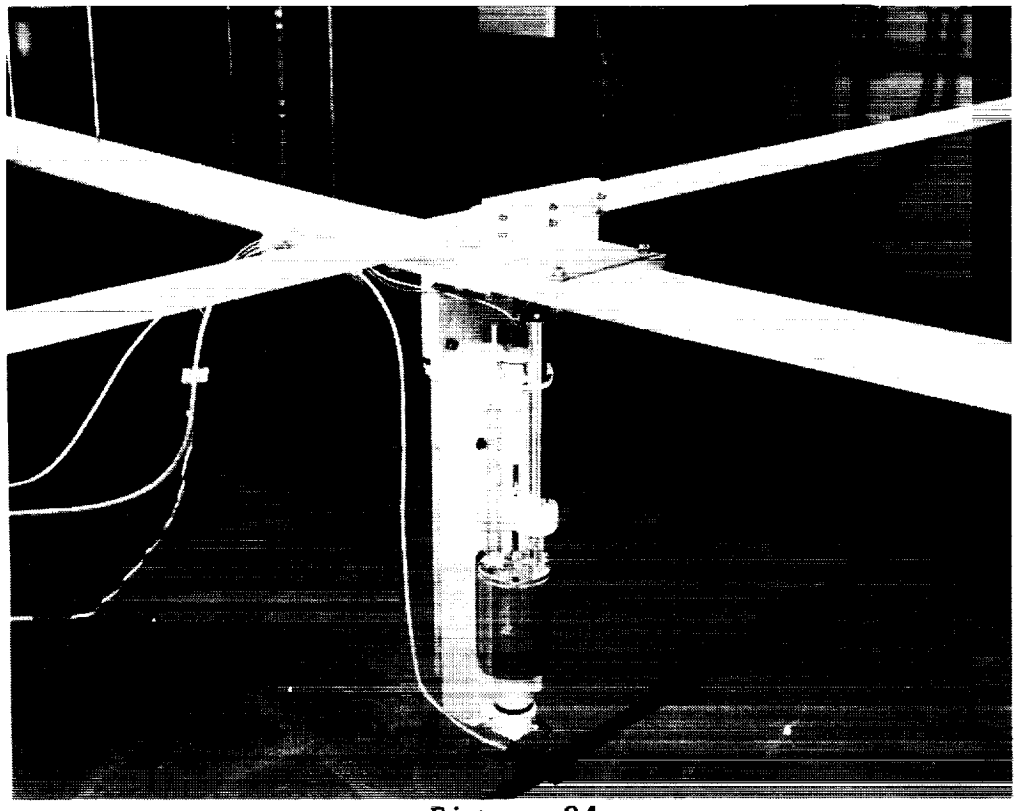

Figure 24

Figure 25 shows the relative to inertial velocity FRF (frequency response function), where the relative velocity is the output of the LVT and the inertial velocity is the integrated output of the accelerometer. The lower pair of curves is for the open-loop case and the upper pair is for the control loop closed case. The smoother curves are the predicted FRFs, and the more jagged curves are the experimental FRFs. The agreement is obviously excellent.

Figure 25 also presents the base force to inertial velocity FRFs. Again, the upper curves are closed loop and the lower open loop. It should be noted that the accelerometer and LVT are accurate down to DC, whereas the force gauges are not. Thus, the predicted and measured values differ at low frequency. Any problems with either the LVT or accelerometer would have been apparent in the relative to inertial velocity FRF.

The resonance at approximately 8.5 Hz, most obvious in the closed-loop measured response in the second plot, is in the experimental setup.

Actuator Transfer Functions

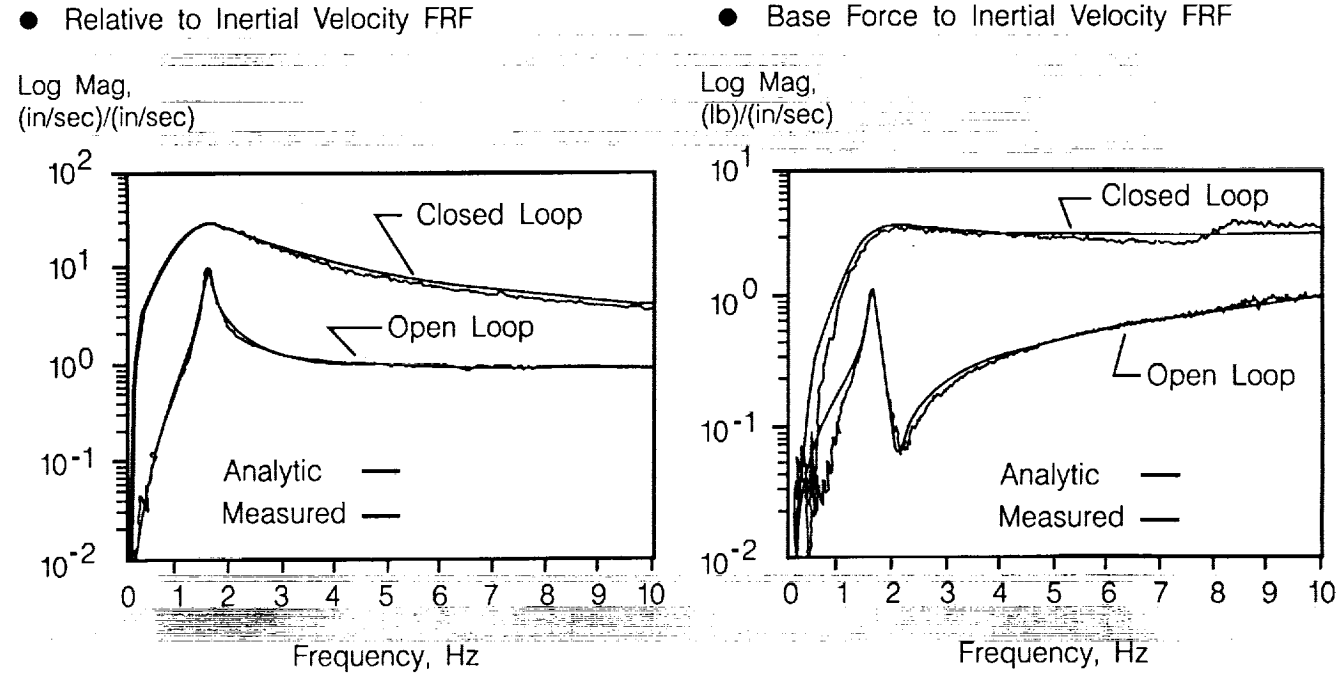

Figure 25

The DTA solar array blanket modes are below one Hz. Thus, they could be destabilized by the 1.5 Hz actuators. However, analysis showed that the blanket mode motion is almost totally in a horizontal plane and thus should not be observable to the actuator accelerometers, which have their sensitive axes vertical in the installed configuration. To provide additional confidence in the analysis, a simple undamped cruciform structure was fabricated and damped actively.

The cruciform beam experiment is shown in Figure 26. The larger beam vibrates vertically in its first mode at a frequency approximating the DTA mode targeted for active augmentation. The smaller beam vibrates horizontally in its first mode at approximately the DTA solar array blanket mode frequency.

This simple test was performed successfully. Approximately 30 percent active modal viscous damping was given to the 32 lb. beam by the actuator, and predicted performance matched measured results nearly perfectly.

Cruciform Beam Experiment

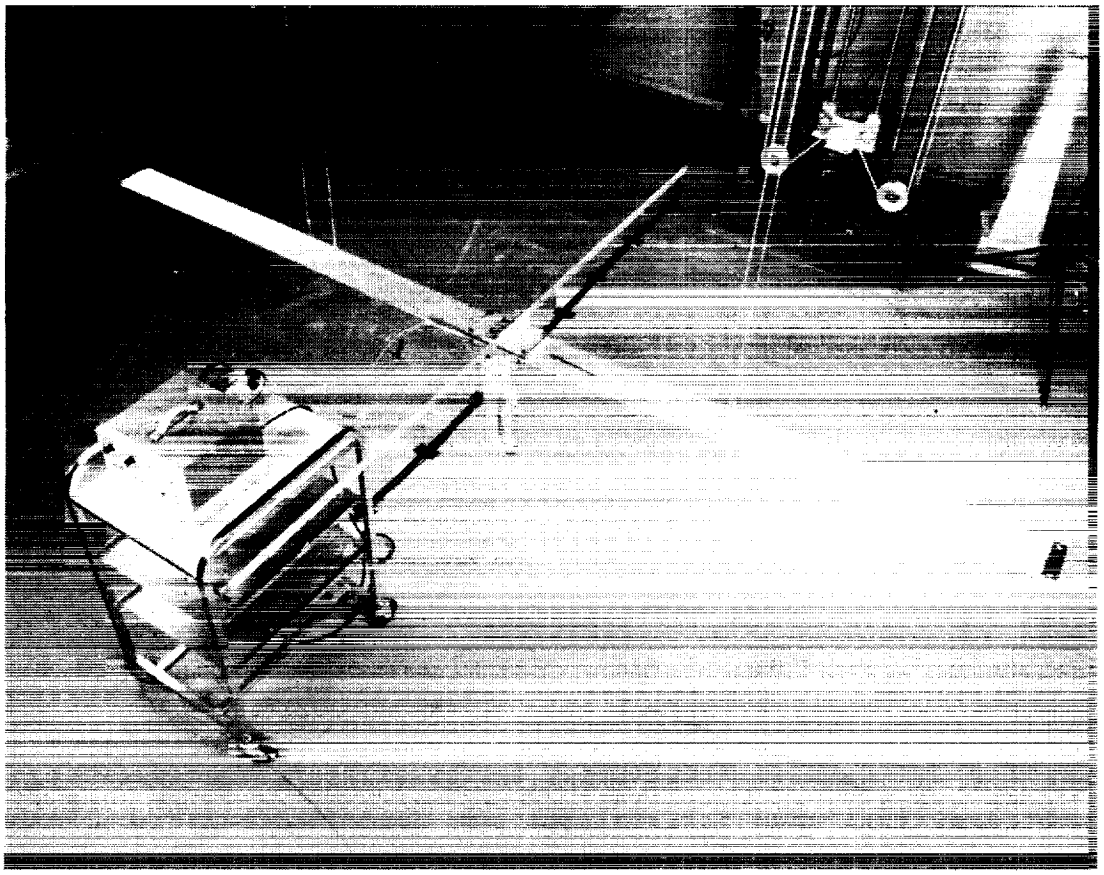

Figure 26

The DTA was assembled for a program review following the Second NASA/DoD CSI Conference. This activity provided a final fit check of all components. The assembled DTA is shown in Figure 27.

Assembled DTA

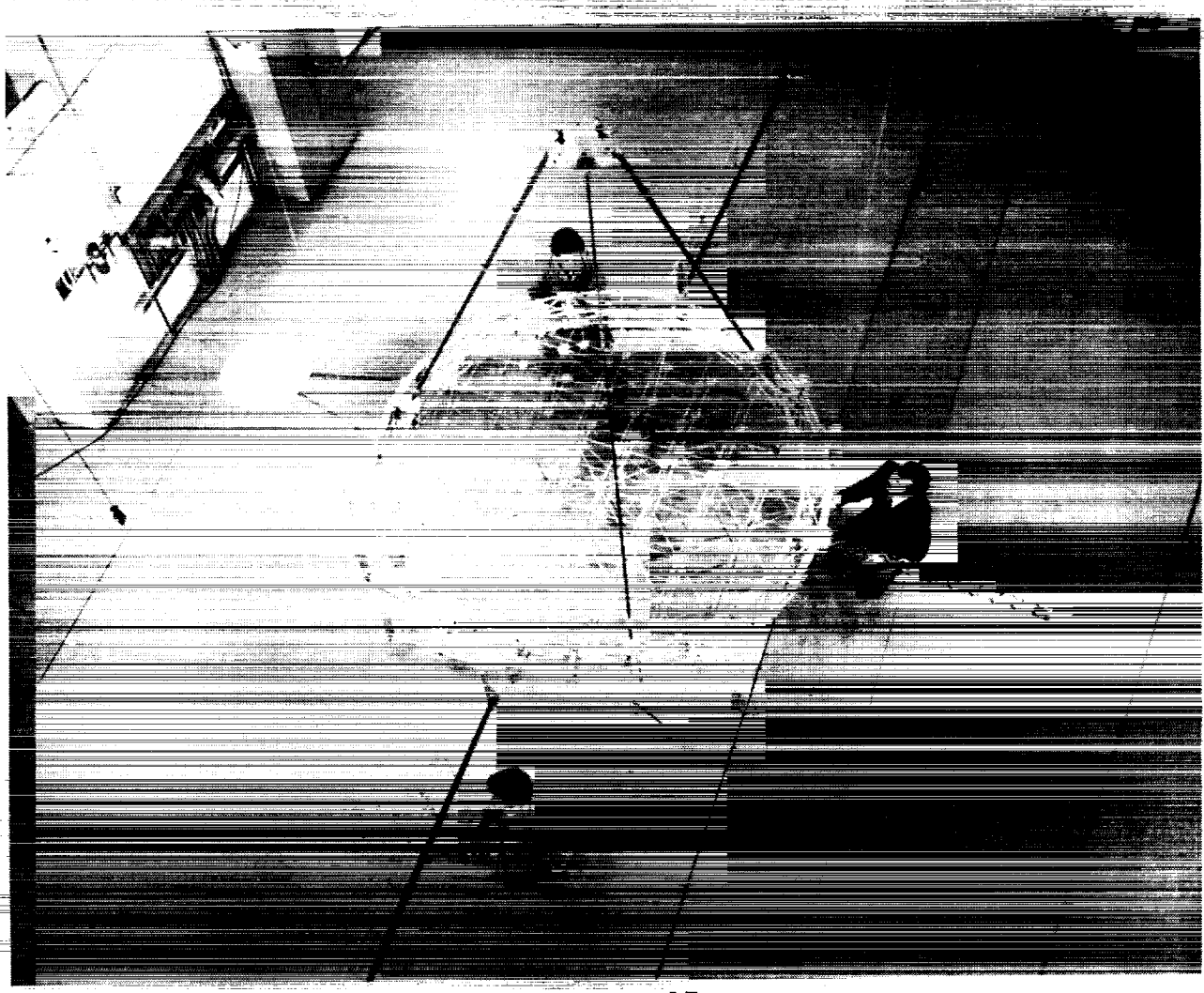

Figure 27

ORIGINAL PAGE
BLACK AND WHITE PHOTOGRAPH

The DTA was assembled, the modal control system was installed, and open- and closed-loop testing were performed. Figure 28 shows the test article in a specially constructed test chamber, which provided a quiet, temperature-controlled environment. The suspension techniques were identical to those used for the ring truss modal survey, although the suspension cables were somewhat shorter.

Several test methods were investigated. Multi-point burst random modal test techniques were chosen as most appropriate for this structure. As many as four simultaneous drive points were used, with a total of five different setups. In addition, sine sweep tests were run to provide data for comparison with those obtained during burst random testing.

DTA in Test Chamber

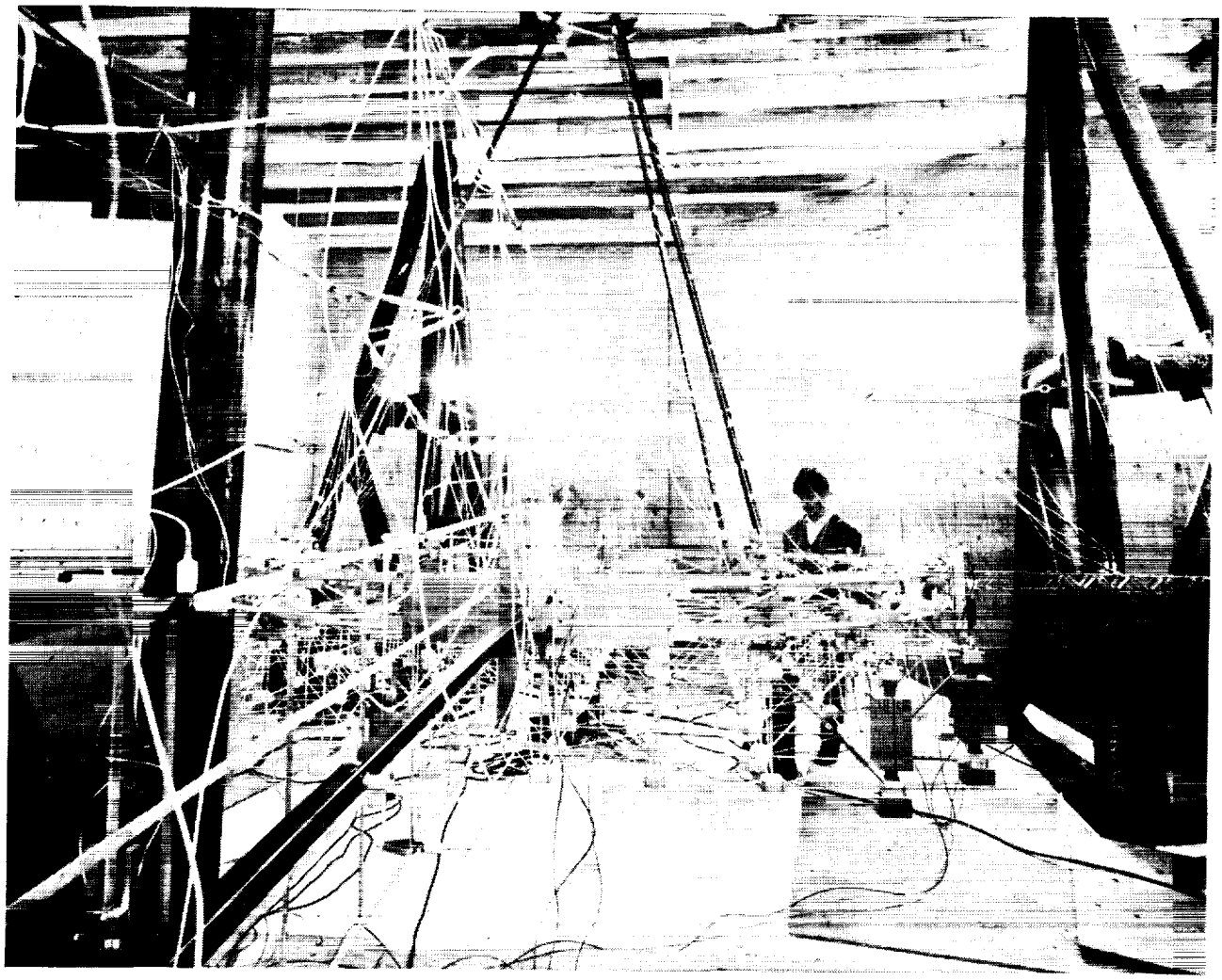

Figure 28

Approximately 200 channels of data were obtained for each drive point. Figure 29 shows a comparison between one measured and two analytic FRFs from the open-loop tests. The sharp curve shows the response of the tip of a solar array to a vertical excitation at the solar array mast tip, assuming the 0.2 percent modal damping found during the ring truss modal survey to be characteristic of an untreated structure of this type. The second curve shows the corresponding FRF with the predicted levels of passive modal damping from the coupled model. The third curve shows the measured FRF. There are some obvious differences, but the agreement is generally very good. We note that the general trend is to underpredict the passive damping level.

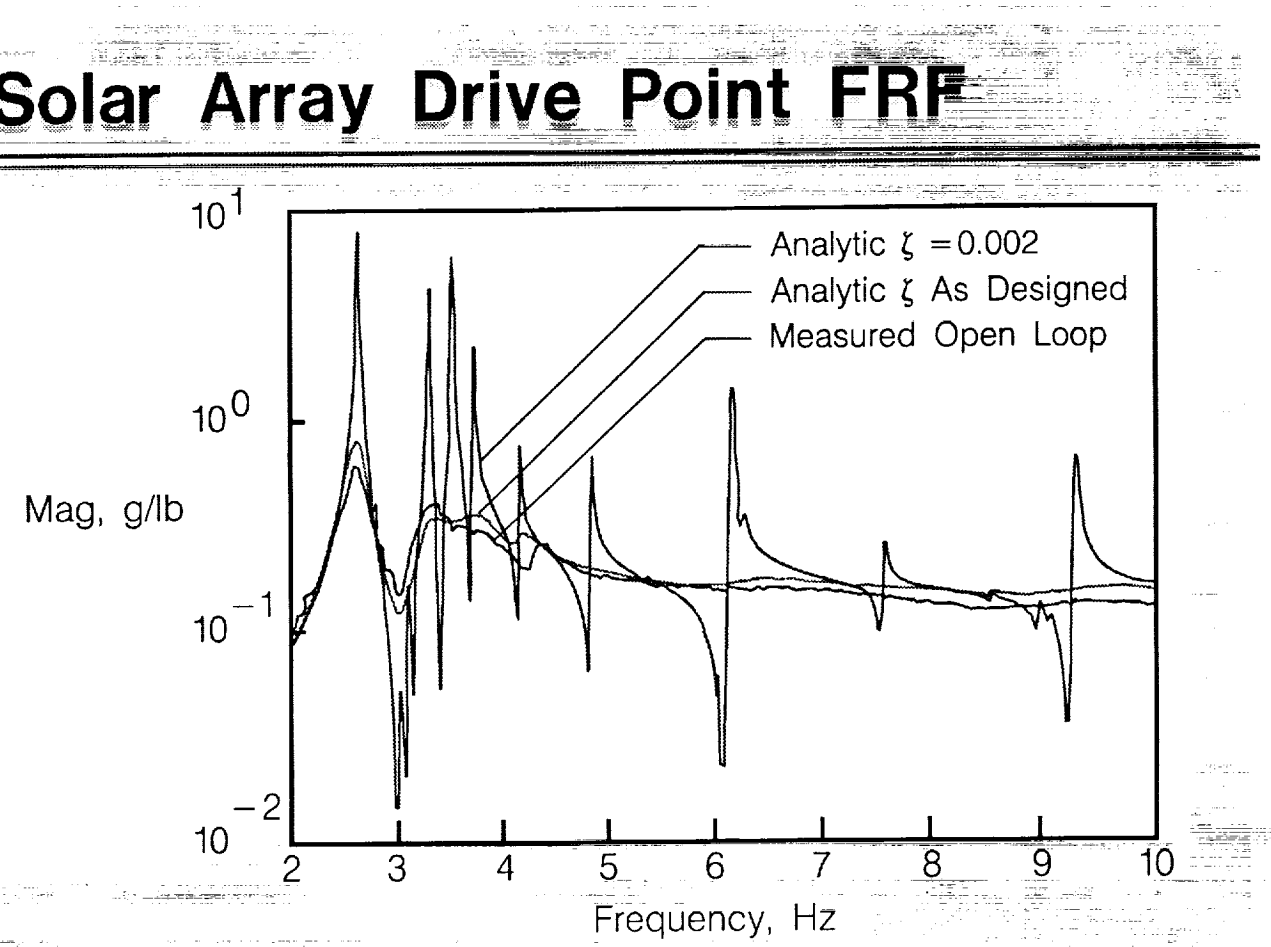

Figure 29

Figure 30 displays the results of open loop tests compared with analytic results. Corrections have been made for VEM frequency effects and the effects of geometric stiffness and the deformed shape of the structure due to the one-g loading.

The high modal density of heavily damped modes (40 modes below 10 Hz) and experimental noise due to the low frequencies and low excitation levels resulted in a challenging parameter identification problem. Modal analysis requires curve fits of the experimental data, and the damping levels identified by apparently equally good attempts would frequently vary by 20 percent, i.e., if the mean value of damping for a given mode was found to be 10 percent, apparently equally good curve fits would produce results between 8 percent and 12 percent.

Most of these results fall within the 20 percent band of parameter identification uncertainty.

DTA Open-Loop Global Modes

System Mode	Global Mode	f, Hz		ζ, %	
		Test	Analytic	Test *	Analytic
15	1	2.61	2.61	3.6	2.8
20	2	3.25	3.29	5.0	4.4
21	3	3.53	3.50	8.8	8.2
22	4	3.72	3.70	5.2	4.7
26	5	4.83	4.60	4.5	7.8
27	6	5.04	4.81	11.4	10.4
35	7	6.48	6.12	12.7	10.0
37	8	9.40	7.52	10.3	6.0
42	9	8.92	9.04	7.0	6.8
45	10	9.26	9.28	8.6	7.0

* Accuracy Approximately ± 20%

Figure 30

Figure 31 shows the open-loop FRF previously shown in Figure 29 and the corresponding measured FRF for the closed-loop system. The global mode at approximately 2.5 Hz was targeted for active damping augmentation. The effect of the active damping is noticeable at the targeted resonance, but has relatively small effect at other frequencies.

Solar Array Drive Point FRF

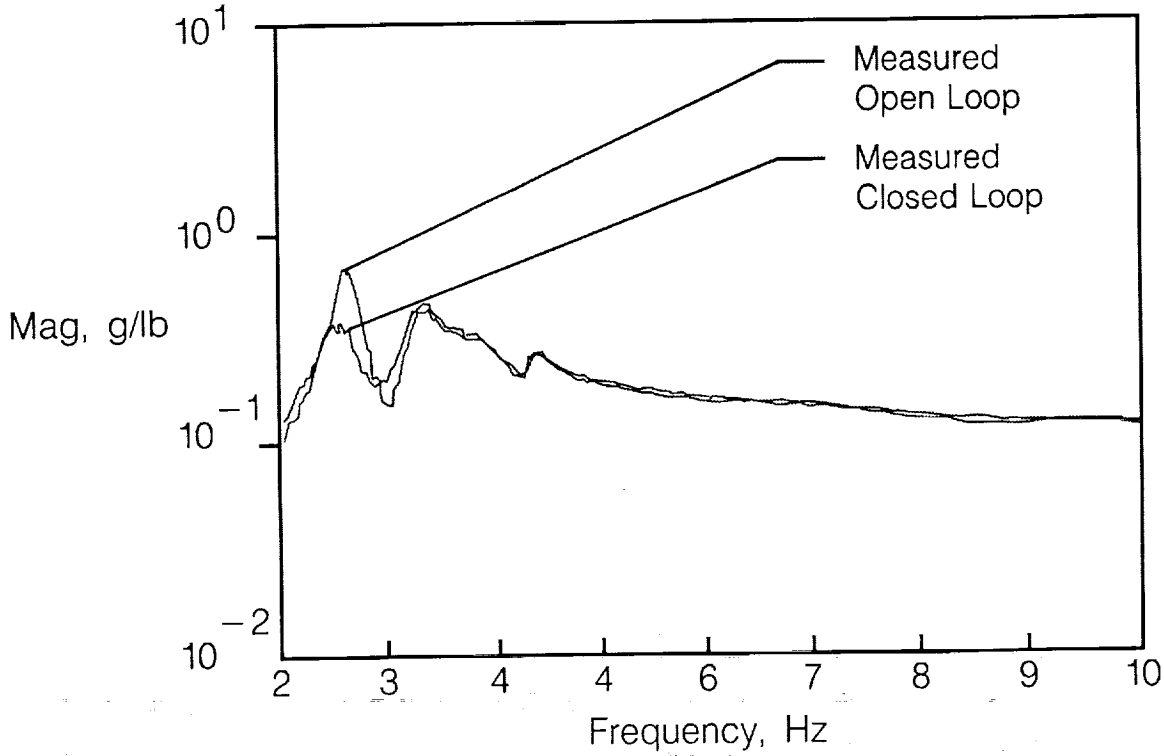

Figure 31

Figure 32 shows the analytic and measured results for the modes which received significant damping from the active augmentation. The agreement between predicted and measured values is excellent. We note, however, that the same 20 percent band as in the open-loop case must be applied to the experimental damping levels.

DTA Closed-Loop Global Modes

	Global Mode +	f, Hz		ζ, %	
		Test	Analytic	Test *	Analytic
Open Loop	1	2.61	2.61	3.6	2.8
	6	5.04	4.81	11.4	10.4
	7	6.48	6.12	12.7	10.0
	10	9.26	9.28	8.6	7.0
Closed Loop	1	2.55	2.54	7.5	8.4
	6	5.00	4.68	15.0	15.8
	7	6.40	5.98	17.0	18.2
	10	9.30	9.30	13.0	12.0

+ Other Modes Not Appreciably Affected by Active Damping

* Accuracy Approximately ± 20%

Figure 32

Several important conclusions can be drawn from work performed on the PACOSS program. Most importantly, the best technique for control of large, flexible space structures is a combination of passive and active control. Passive augmentation is critical because the inherent damping in untreated precision structures is very small and unpredictable. It is possible, however, to design significant, predictable levels of passive damping into large space structures. Finally, the effects of active augmentation of a passively damped structure are predictable, due in large part to the benign nature of the passively damped structure. (Fig. 33.)

Conclusions

- Best LSS Control Strategy a Combination of Passive and Active
- It Is Possible To Design a Predictable Amount of Passive Damping Into a Structure
- DTA Open and Closed-Loop Properties Predictable

Figure 33

REFERENCES

1. Gehling, R. N.: Active Augmentation of a Passively Damped Representative Large Space System. Damping 1986 Proceedings, May 1986, (AFWAL-TR-86-3059)

2. Richards, K. E., and Rogers, L. C.: PACOSS Program Overview and Status. NASA/DOD Control/Structures Interaction Technology 1986 (NASA Conference Publication 2447)

3. Morgenthaler, D. R., and Gehling, R. N.: Design and Analysis of the PACOSS Representative System. Damping 1986 Proceedings, May 1986, (AFWAL-TR-86-3059)

4. Morgenthaler, D. R.: Design and Analysis of Passively Damped Large Space Structures. ASME Publication DE-Vol. 5, The Roll of Damping in Vibration and Noise Control, September, 1987.

5. Gehling, R. N.: Large Space Structure Damping Treatment Performance: Analytic and Test Results. ASME Publication DE-Vol. 5, The Roll of Damping in Vibration and Noise Control, September, 1987.